PROCEEDINGS, 42nd Workshop on Geothermal Reservoir Engineering
Stanford University, Stanford, California, February 13-15, 2017
SGP-TR-212

Multiscale Elastic-Waveform Inversion for Geothermal Reservoir Characterization

Benxin Chi, Kai Gao and Lianjie Huang

Los Alamos National Laboratory, Geophysics Group, Los Alamos, NM 87545, USA

E-mails: benxinchi@lanl.gov, kaigao@lanl.gov, ljh@lanl.gov

Keywords: Elastic-waveform inversion, multiscale, velocity model, vertical seismic profiling.

ABSTRACT

Accurate subsurface velocity models are crucial for reliable geothermal reservoir characterization. Elastic-waveform inversion (EWI) is a powerful tool for building high-resolution subsurface velocity models with seismic data. However, the conventional single-scale EWI requires a good initial model to avoid converging to local minima of the misfit function. For practical applications, we often can obtain only a low-resolution, approximate initial model that might be significant different from the real velocity model. We develop a novel multiscale EWI method to improve the reliability of velocity inversion for practical applications. Our new method combines a multi-frequency approach in the data domain and a multiscale scheme in the model domain. In the data domain, we apply a frequency bandpass filter to seismic data to obtain data in several frequency bands, and invert seismic data sequentially from a low-frequency band to a high-frequency band. During inversion in each frequency band, we first invert seismic data envelopes for a low-resolution velocity model, and then invert seismic data themselves to further improve the velocity model. In the model domain, we apply the wavelet transform to the velocity inversion result during inversion in each frequency band. We validate our new multiscale EWI method using synthetic vertical seismic profiling data for an elastic model of the Raft River geothermal field, and demonstrate that our new method produces more accurate velocity inversion results compared to the conventional single-scale EWI, particularly when the initial model is very different from the true velocity model.

1. INTRODUCTION

Accurate determination of subsurface medium properties is a great challenge in geothermal reservoir characterization. Elastic-waveform inversion (EWI) has the potential to accurately estimate subsurface geophysical properties by exploiting the full information of prestack seismic data (Tarantola, 1984; Mora, 1987; Virieux and Operto, 2009; Lin and Huang, 2015). EWI aims to minimize the difference between observed and synthetic multicomponent seismic data. However, the inverse problem for EWI is highly nonlinear. If the initial/starting model is very different from the true model, the conventional single-scale EWI easily traps into a local minimum, resulting in an incorrect inversion result.

Different approaches have been developed to alleviate the nonlinearity of EWI and to circumvent the cycle-skipping problem. In the time domain, a multiscale strategy was developed using successively bandpass seismic data from a low frequency band to a high frequency band (Bunks et al., 1995). The frequency domain inversion provides a more natural multiscale framework by performing minimization with successively increasing frequencies (Sirgue and Pratt, 2004). With low frequency data, the number of local minima in EWI is greatly reduced. Therefore, compared to using the full-band seismic data, the multiscale inversion result tends to converge to the global minimum. In seismic tomography, the multiscale inversion strategy has been formulated using wavelet transform. The model is decomposed into a series of wavelets, and a coarse-to-fine multi-resolution representation of the model can then be reconstructed with these wavelets (Loris et al., 2007; Hung et al., 2010; Simons et al., 2011). The multiscale strategy can also be achieved by modifying the objective function of waveform inversion. For example, compared to seismic waveforms, seismic data envelopes contain more low frequency information and consequently, inversion with seismic data envelopes can produce a more reliable low-resolution initial velocity model for EWI to improve the robustness of EWI (Chi et al., 2014).

We develop a novel multiscale EWI method that combines the multiscale strategy in the data domain with the multiscale approach in the model domain. In the data domain, we apply a frequency bandpass filter to both the observed and synthetic data. In each frequency band, we first conduct seismic-envelope inversion, and then perform seismic-waveform inversion. The inversion result of a lower-frequency band data is used as the initial model of inversion with a higher-frequency band data. During inversion at each frequency band, we apply the wavelet transform to the inversion model to obtain an inversion result with a spatial resolution comparable to the frequency band used.

We use synthetic vertical seismic profiling (VSP) data for an elastic model of the Raft River geothermal field (Ayling and Moore, 2013) to validate our new multiscale EWI method. We compare our multiscale inversion results with those obtained using the conventional single-scale EWI, and our results demonstrate that our new multiscale EWI method produces more accurate compressional- and shear-wave velocity models than the latter, particularly when the initial velocity models are significant different from the true models.

2. METHOD

Elastic-waveform envelope inversion can produce a low-resolution initial velocity model for elastic-waveform inversion to improve the convergence. Analog to elastic-waveform inversion, envelope inversion fits data envelope $\mathbf{e}_{\text{obs}}$ with synthetic data envelope $\mathbf{e}_{\text{cal}}$:

$$E(\mathbf{m}) = 1 - \frac{\int \mathbf{e}_{\text{obs}}(t)\mathbf{e}_{\text{cal}}(t)\,dt}{\sqrt{\int \mathbf{e}_{\text{obs}}^2(t)\,dt}\sqrt{\int \mathbf{e}_{\text{cal}}^2(t)\,dt}}. \tag{1}$$

Elastic-waveform inversion progressively fits synthetic elastic waveforms $\mathbf{d}_{\text{cal}}$ with recorded elastic waveforms $\mathbf{d}_{\text{obs}}$ to obtain elastic parameters $\mathbf{m}$. We pose this inversion as the minimization of the following zero-lag cross-correlation objective function:

$$E(\mathbf{m}) = 1 - \frac{\int \mathbf{d}_{\text{obs}}(t)\mathbf{d}_{\text{cal}}(t)\,dt}{\sqrt{\int \mathbf{d}_{\text{obs}}^2(t)\,dt}\sqrt{\int \mathbf{d}_{\text{cal}}^2(t)\,dt}}. \tag{2}$$

The correlation-based misfit can suppress some inversion artifacts caused by the difficulty in matching amplitudes of seismic waveforms in practical applications. Synthetic elastic-waveforms $\mathbf{d}_{\text{cal}}$ are related to model parameters $\mathbf{m}$ as

$$\mathbf{d}_{\text{cal}} = f(\mathbf{m}), \tag{3}$$

where f is the wavefield propagation operator. We simulate elastic-wave propagation using an optimized high-order staggered-grid finite-difference algorithm with the convolutional perfectly matched layers (Tan and Huang, 2014a; Tan and Huang, 2014b).

Data-domain multiscale full-waveform inversion was developed by Bunks et al. (1995). Low-frequency bandpassed data are used at earlier stages of inversion, producing a long-wavelength model. The inverted model is then used as the initial model at later stages of inversion to produce a short-wavelength/high-resolution model. With gradually increased frequency bands, all frequency contents of the observed data are eventually used for inversion. The objective function of this data-domain multiscale approach can be defined as:

$$E_m(\mathbf{m}) = 1 - \frac{\int W(\omega)\mathbf{d}_{\text{obs}}(t)W(\omega)\mathbf{d}_{\text{cal}}(t)\,dt}{\sqrt{\int \left[W(\omega)\mathbf{d}_{\text{obs}}(t)\right]^2 dt}\sqrt{\int \left[W(\omega)\mathbf{d}_{\text{cal}}(t)\right]^2 dt}}, \tag{4}$$

with the frequency-dependent weights defined as

$$W(\omega) = \begin{cases} 1, & \text{if } \omega_{\min} \le \omega \le \omega_{\max} \\ 0, & \text{if } \omega > \omega_{\min} \text{ or } \omega < \omega_{\max} \end{cases}, \tag{5}$$

where $\omega_{\min}$ and $\omega_{\max}$ are the minimum and maximum frequency of a frequency band, respectively. In the time domain EWI, this scheme is implemented by filtering observed and synthetic data before the gradient computation using the adjoint-state method (Plessix, 2006).

Different frequency band of data should invert for different spatial resolution of models. The inversion model can be transformed into different spatial scales using the wavelet transform:

$$X = W\mathbf{m}, \tag{6}$$

where X denotes the wavelet transform result of the inversion model, and W is the wavelet basis. Reconstruction of the model $\mathbf{m}_{\text{reconstr}}$ is obtained using the inverse wavelet transform:

$$\mathbf{m}_{\text{reconstr}} = W^T X = W^T W\mathbf{m}. \tag{7}$$

With Equations (6) and (7), we can obtain multiscale model representations. In our joint data-domain and model-domain multiscale inversion, we employ coarser scales coefficients at earlier stages (low frequencies) of EWI, and gradually add finer scales at later stages of EWI.

3. NUMERICAL EXAMPLES

We use synthetic VSP data for an elastic model of the Raft River geothermal field as shown in Figure 1 to demonstrate the capability of our new multiscale elastic-waveform inversion method. The model contains a vertical Narrows zone. Synthetic VSP data are generated using 42 sources evenly distributed along the surface of the model with a spatial interval of 60 m, and 115 receivers along a borehole as indicated by the black curve in Figure 1. The receivers are located between 0.5 km and 1.8 km in depth. A Ricker wavelet with a dominant frequency of 30 Hz is used as the source function.

We study the capability of our new multiscale EWI using different starting models. In the first example, we smooth the original velocity models in Figure 1 by averaging the slowness within two wavelengths at the dominant frequency of the source wavelet, resulting in the smoothed models in Figure 2. We use these smoothed models as the starting models for EWI. Figure 3 shows the results of single-scale and multiscale EWI. For this relatively good starting model, we find that the improvement of multiscale EWI is not significant (Figure 3). Both the single-scale and multiscale strategy can obtain reasonable inversion results, as demonstrated by the quantitative comparisons among model updates in Figure 4. Nevertheless, the convergence curves in Figure 5 show that the multiscale EWI converges faster than the single-scale EWI. The multiscale inversion further decreases the data misfit by 20% and the model misfit by 30%.

In the second example, we smooth the original velocity models in Figure 1 by averaging the slowness within four wavelengths at the dominant frequency of the source wavelet to generate a relatively poor initial model in Figure 6. Figure 7 shows the results of EWI inversion using the single-scale and multiscale approaches. A quantitative comparison among model updates with those of the initial and true models (Figure 8) validates that our new multiscale inversion method gives more accurate velocity values than the single-scale inversion. Our new method eliminates almost all of the high wavenumber oscillations in the different layers. We plot both the data misfit and the model misfit convergence curves in Figure 9. As in the first example, the multiscale EWI converges faster than the single-scale inversion, and further decreases 60% of the data misfit and 50% of the model misfit from those for the single-scale inversion.

For practical applications, we cannot obtain an accurate starting model, and the starting model is often significant different from the true model. Therefore, we use a model smoothed by averaging the slowness of the original model within eight wavelengths at the dominant frequency of the source wavelet as the initial model (Figure 10). The single-scale EWI produces velocity models with significant inversion artifacts in the shallow regions. In addition, the inversion can barely recover the left and right boundaries of the Narrows zone, as shown in Figure 11. In contrast, our multiscale EWI well reconstructs the shallow layers and the lateral boundaries of the Narrows zone. These findings are also verified in quantitative comparisons of the inversion results in Figure 12. Figure 13 depicts that our multiscale EWI further reduces the data misfit by more than 90% from that of the single-scale EWI.

4. CONCLUSIONS

We have developed a novel elastic-waveform inversion method using multiscale approaches in both data and model domains. At each stage of the inversion process, we apply a frequency bandpass filter to seismic data, and invert different subsets of seismic data from a low-frequency band to a high-frequency band. At the same time, we apply the wavelet transform to the inversion model to obtain an inversion result with a spatial resolution comparable to the frequency band of data used. Our elastic-waveform inversion results of synthetic VSP data for the Raft River geothermal velocity model demonstrate that our new method significantly improves the convergence of elastic velocity inversion compared to the conventional single-scale inversion, particularly for poor initial velocity models.

5. ACKNOWLEDGEMENTS

This work was supported by the Geothermal Technologies Office (GTO) of the U.S. Department of Energy through contract DE-AC52-06NA25396 to Los Alamos National Laboratory. We thank strong support of GTO Program Managers Sean Porse, Zachary Frone, Lauren Boyd, and Holly Thomas. We thank John Queen and Joseph Moore for providing the Raft River geophysical model. The computation was performed on super-computers provided by the Institutional Computing Program of Los Alamos National Laboratory.

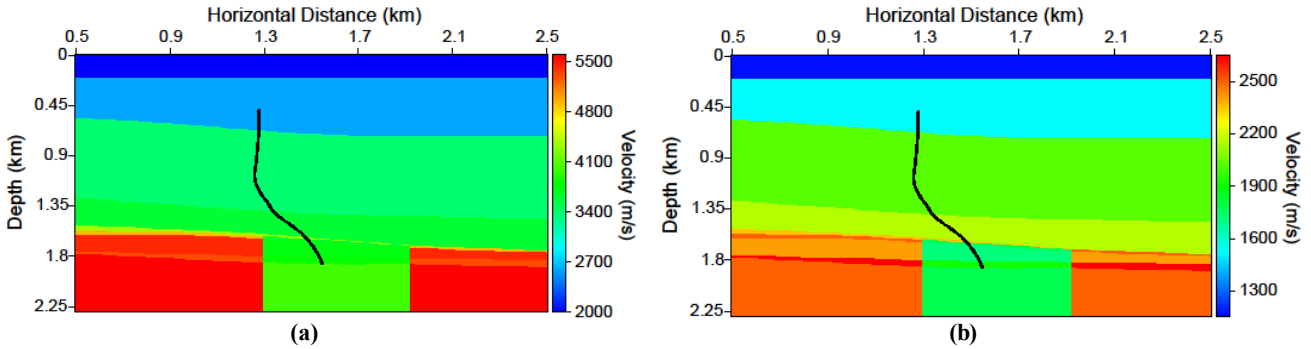

Figure 1: True velocity models built for the Raft River geothermal field: (a) compressional-wave velocity, (b) shear-wave velocity. The black curve indicates the location of the VSP well.

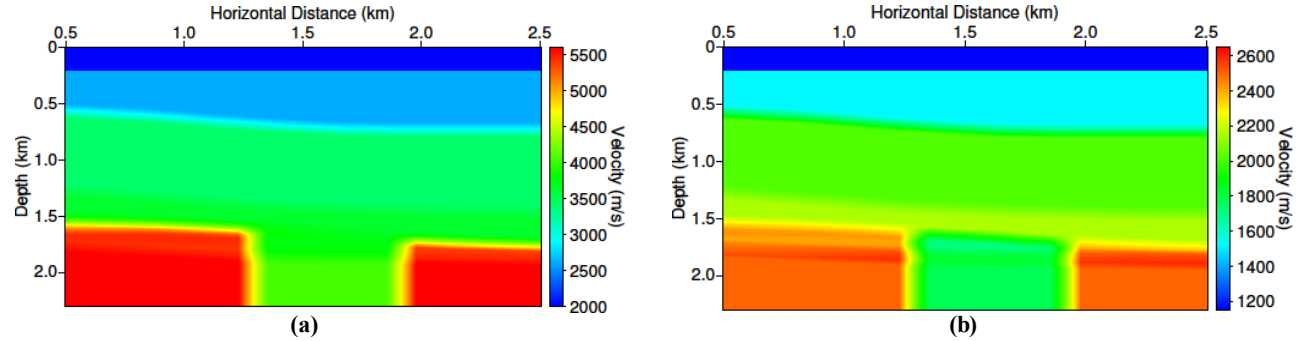

Figure 2: Two-wavelength smoothed velocity models used as the starting models for elastic-waveform inversion: (a) compressional-wave velocity, (b) shear-wave velocity.

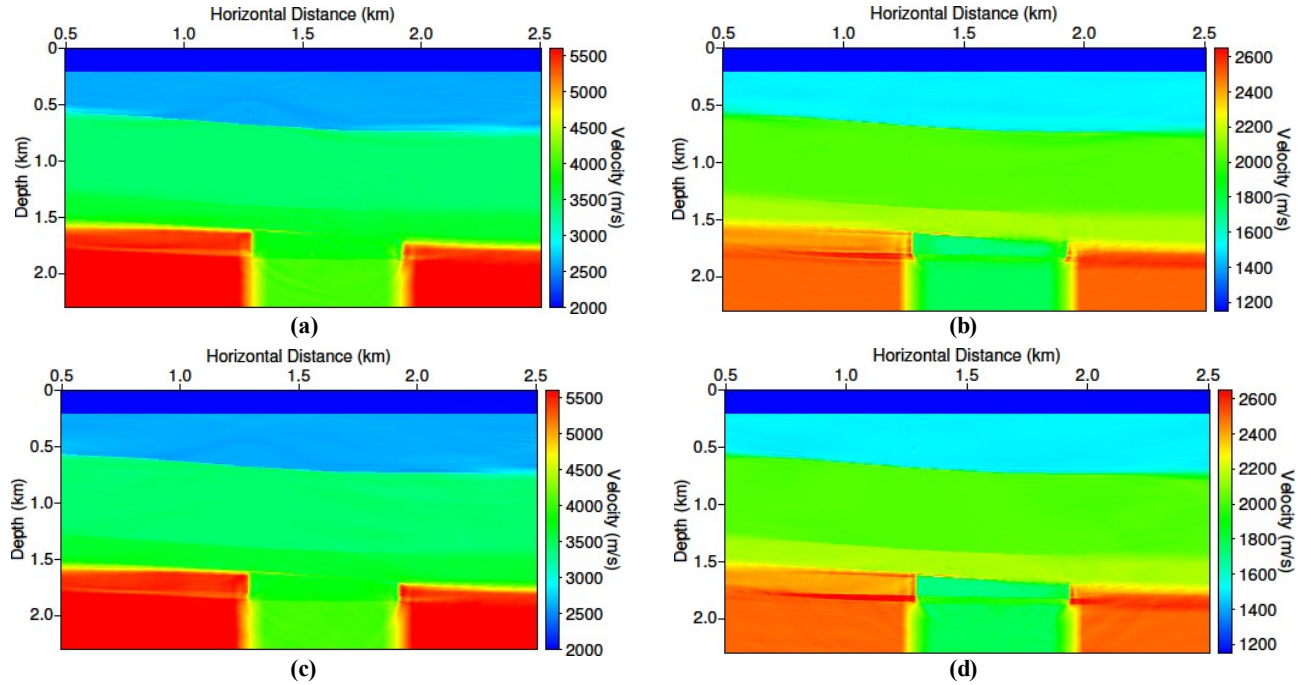

Figure 3: Inverted models obtained with single-scale EWI: (a) compressional-wave velocity, (b) shear-wave velocity; Velocity models obtained with multiscale EWI: (c) compressional-wave velocity, (d) shear-wave velocity.

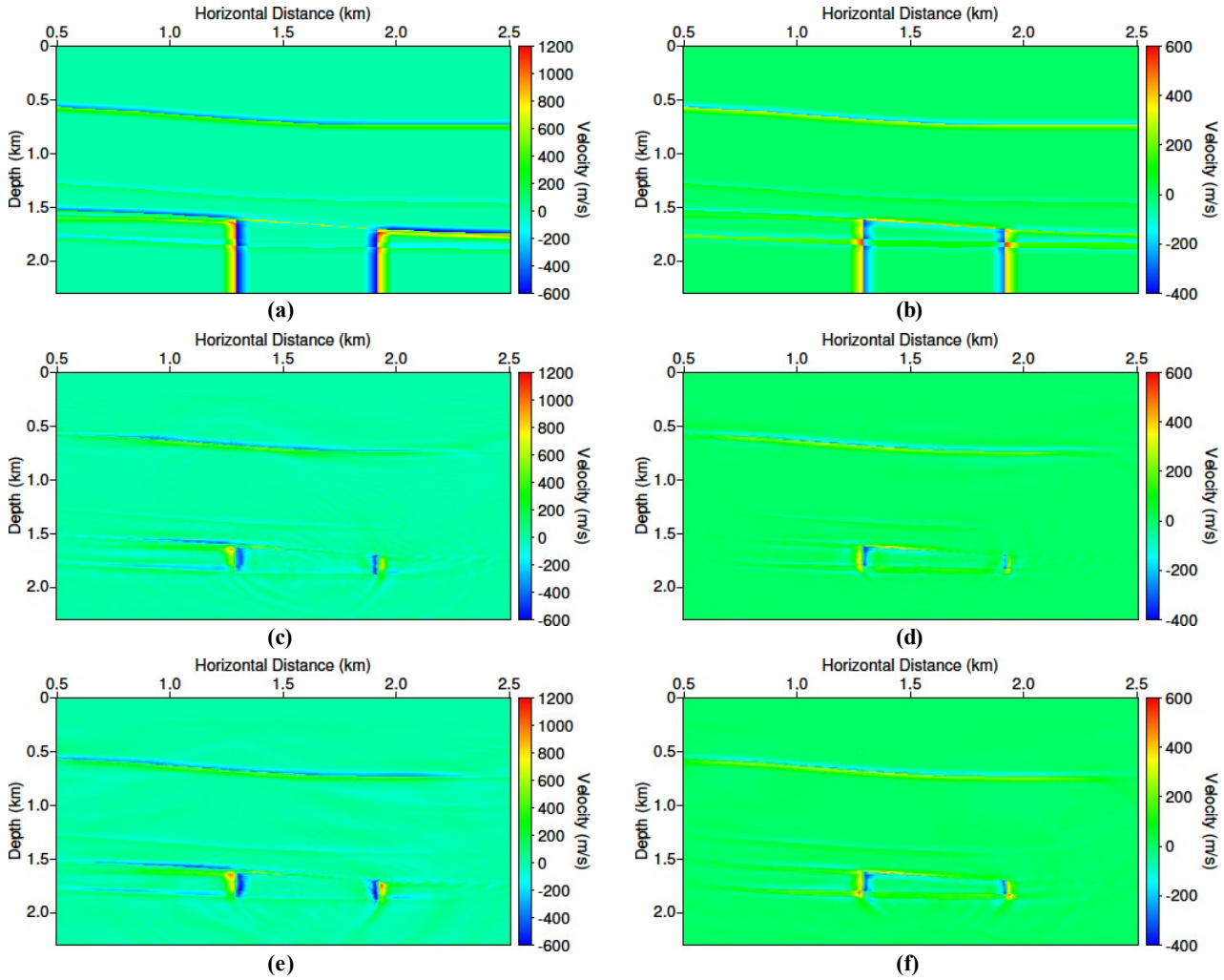

Figure 4: Velocity difference between true and starting models: (a) compressional-wave velocity difference, (b) shear-wave velocity difference; Velocity updates using single-scale elastic-waveform inversion: (c) compressional-wave velocity, (d) shear-wave velocity; Velocity updates using multiscale elastic-waveform inversion: (e) compressional-wave velocity, (f) shear-wave velocity.

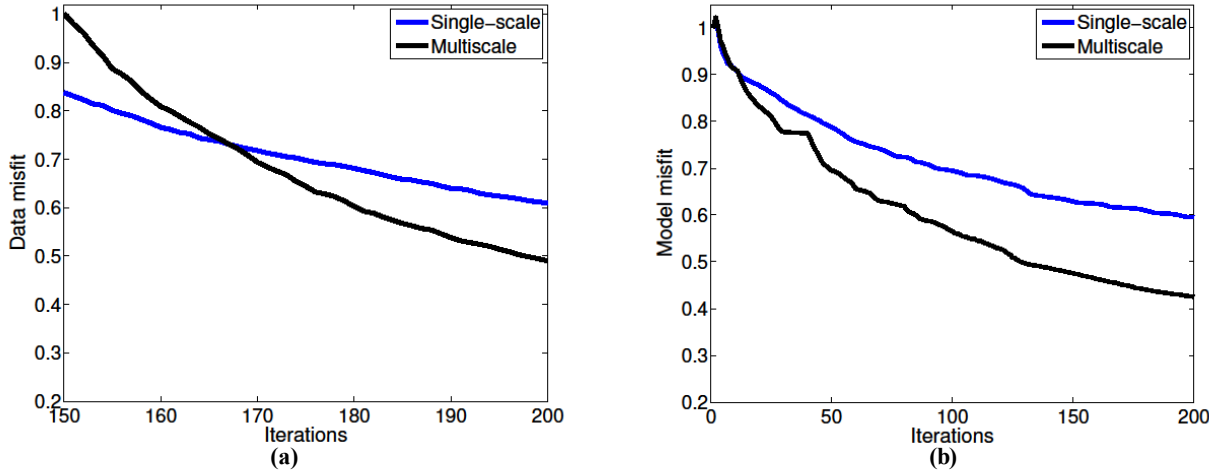

Figure 5: Convergence curves of (a) the normalized data misfit and (b) the normalized model misfit for single-scale EWI (blue line) and multiscale EWI (black line).

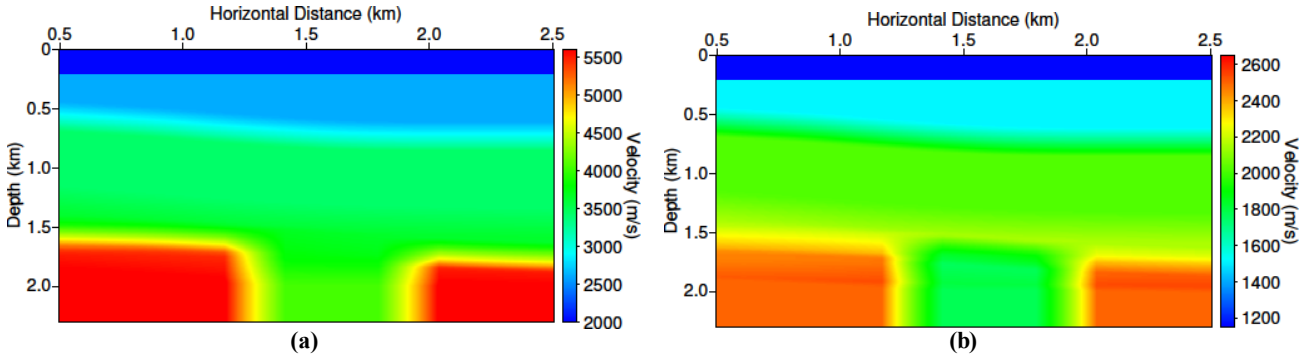

Figure 6: Four-wavelength smoothed velocity models used as the starting models for elastic-waveform inversion: (a) compressional-wave velocity, (b) shear-wave velocity.

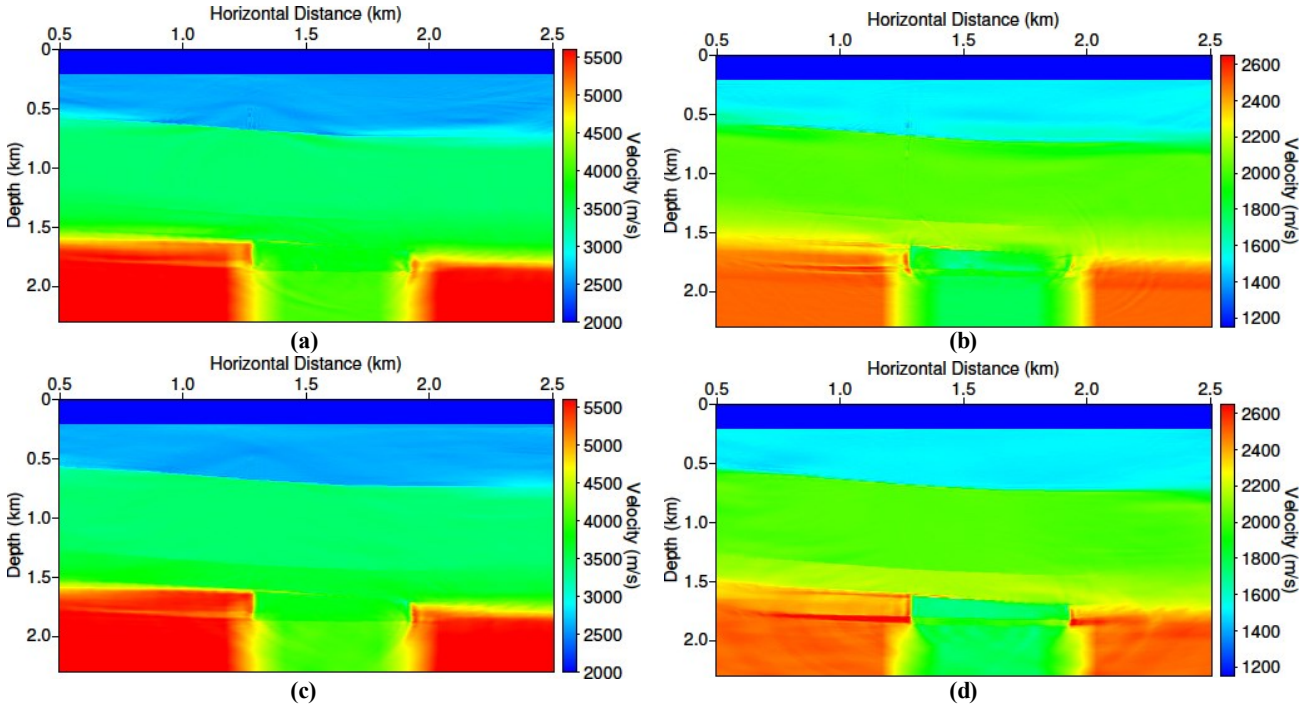

Figure 7: Inverted models obtained with single-scale EWI: (a) compressional-wave velocity, (b) shear-wave velocity; Velocity models obtained with multiscale EWI: (c) compressional-wave velocity, (d) shear-wave velocity.

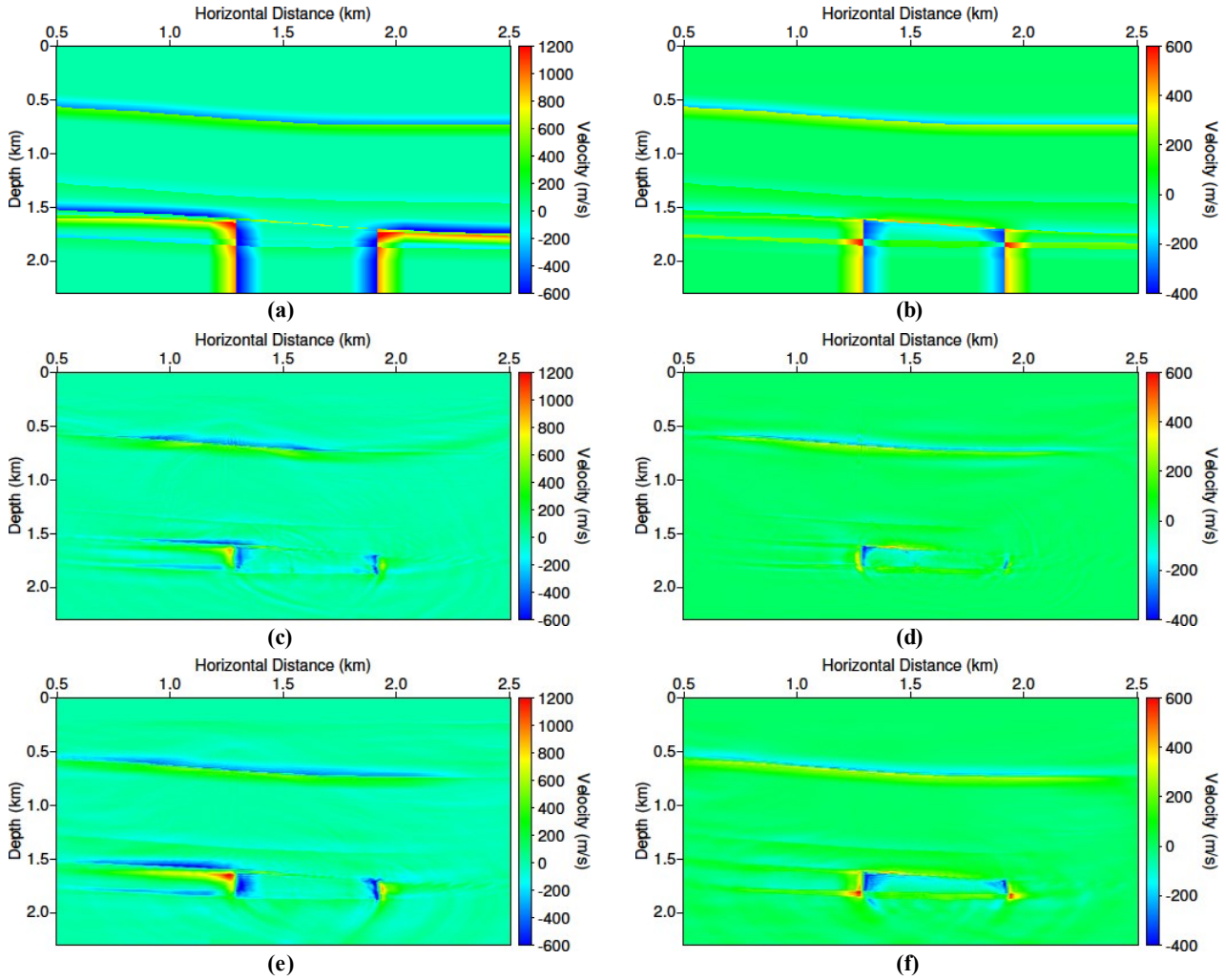

Figure 8: Velocity difference between true and starting models: (a) compressional-wave velocity difference, (b) shear-wave velocity difference; Velocity updates using single-scale elastic-waveform inversion: (c) compressional-wave velocity, (d) shear-wave velocity; Velocity updates using multiscale elastic-waveform inversion: (e) compressional-wave velocity, (f) shear-wave velocity.

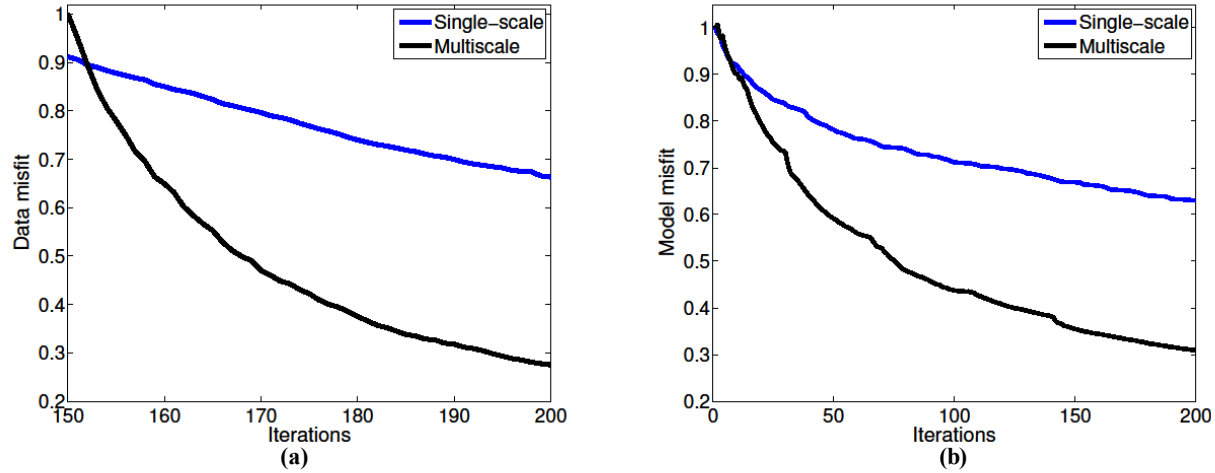

Figure 9: Convergence curves of (a) the normalized data misfit and (b) the normalized model misfit for single-scale EWI (blue line) and multiscale EWI (black line).

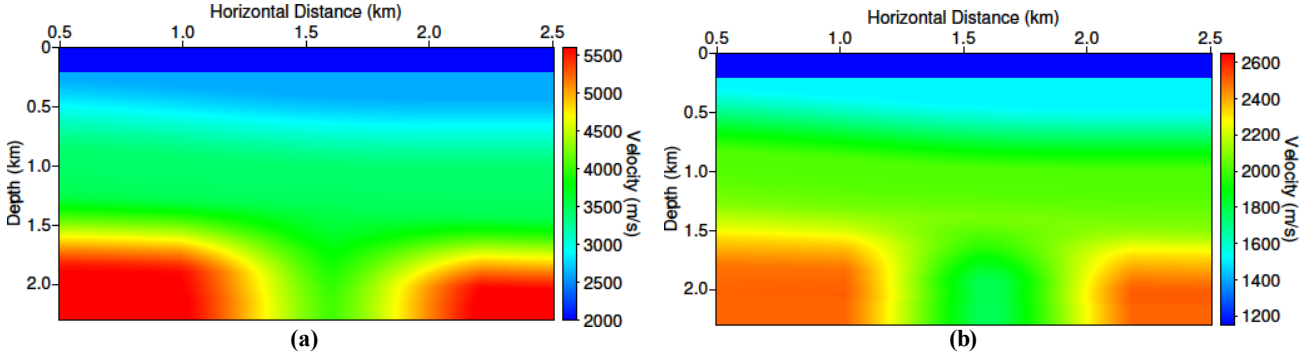

Figure 10: Eight-wavelength smoothed velocity models used as the starting models for elastic-waveform inversion: (a) compressional-wave velocity, (b) shear-wave velocity.

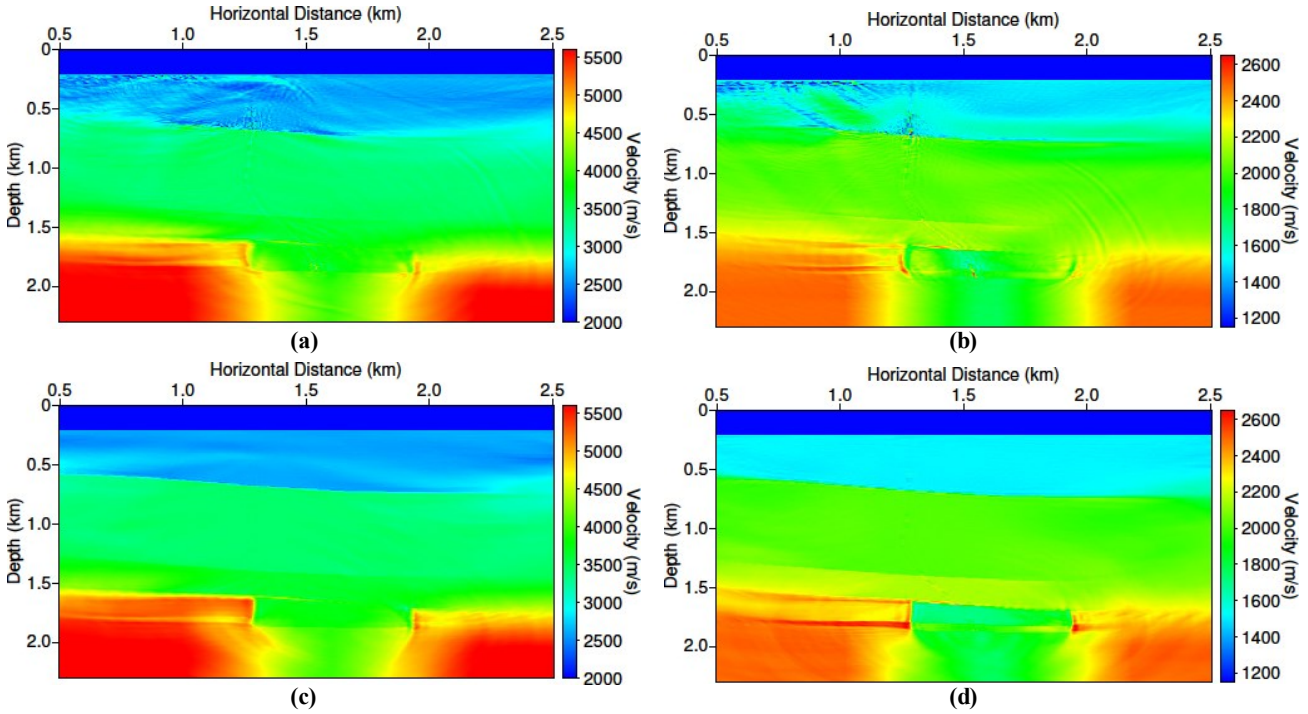

Figure 11: Inverted models obtained with single-scale EWI: (a) compressional-wave velocity, (b) shear-wave velocity; models obtained with multiscale EWI: (c) compressional-wave velocity, (d) shear-wave velocity.

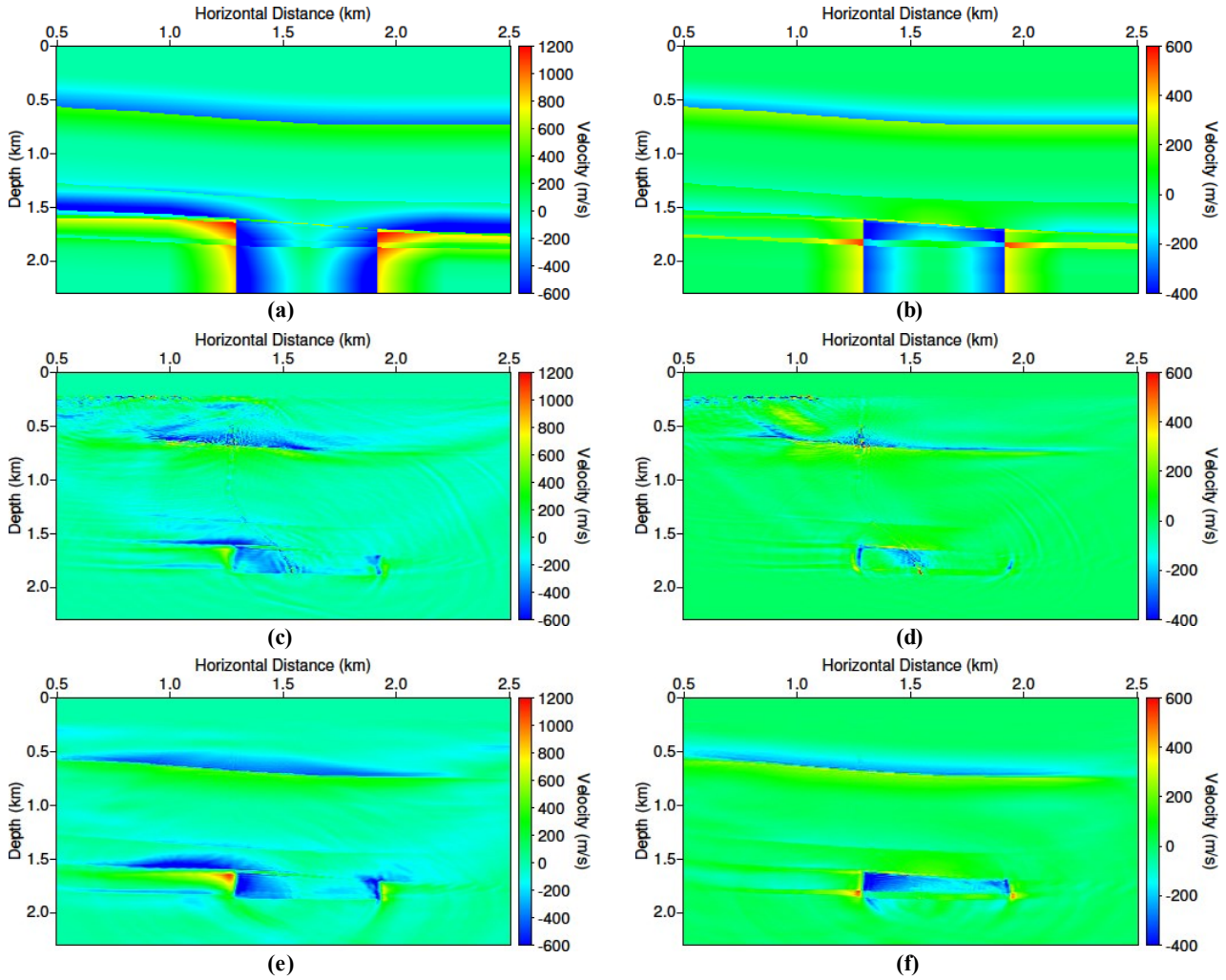

Figure 12: Velocity difference between true and starting models: (a) compressional-wave velocity difference, (b) shear-wave velocity difference; Velocity updates using single-scale elastic-waveform inversion: (c) compressional-wave velocity, (d) shear-wave velocity; Velocity updates using multiscale elastic-waveform inversion: (e) compressional-wave velocity, (f) shear-wave velocity.

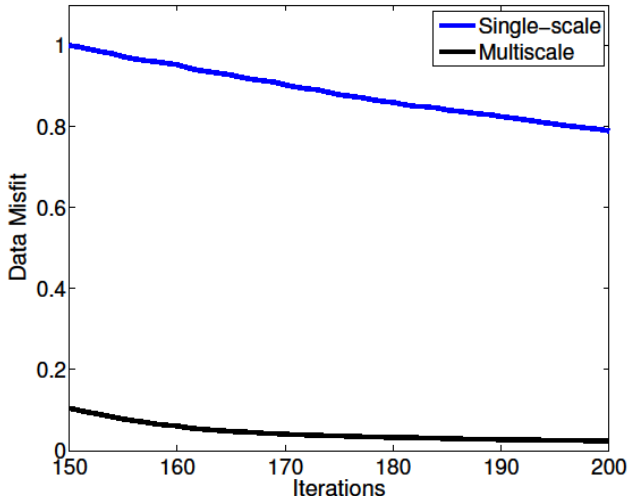

Figure 13: Convergence curves of the normalized data misfit for single-scale EWI (blue line) and multiscale EWI (black line).

REFERENCES

Ayling, B., and Moore, J.: Fluid geochemistry at the Raft River geothermal field, Idaho, USA: New data and hydrogeological implications, *Geothermics*, **47**, (2013), 116-126.

Bunks, C., F. M. Saleck, S. Zaleski, and G. Chavent: Multiscale seismic waveform inversion, *Geophysics*, **60**(5), (1995), 1457-1473.

Chi, B., L. Dong and Y. Liu: Full waveform inversion method using envelope objective function without low frequency data, *Journal of Applied Geophysics*, **109**, (2014), 36-46.

Hung, S.-H., W.-P. Chen, L.-Y. Chiao, and T.-L. Tseng: First multiscale, finite-frequency tomography illuminates 3D anatomy of the Tibetan Plateau: *Geophysical Research Letters*, **37**, (2010), L06304.

Lin, Y., and L. Huang: Acoustic- and Elastic-waveform inversion using a modified total-variation regularization scheme, *Geophysical Journal International*, **200**, (2015), 489-502.

Loris, I., G. Nolet, I. Daubechies, and F. A. Dahlen: Tomographic inversion using L1-norm regularization of wavelet coefficients, *Geophysical Journal International*, **170**, (2007), 359–370.

Mora, P.: Nonlinear two-dimensional elastic inversion of multioffset seismic data, *Geophysics*, **52**(9), (1987), 1211-1228.

Plessix, R.-E.: A review of the adjoint-state method for computing the gradient of a functional with geophysical applications, *Geophysical Journal International*, **167**, (2006), 495–503.

Simons, F. J., I. Loris, G. Nolet, I. C. Daubechies, S. Voronin, J. S. Judd, P. A. Vetter, J. Charlety, and C. Vonesch: Solving or resolving global tomographic models with spherical wavelets, and the scale and sparsity of seismic heterogeneity, *Geophysical Journal International*, **187**, (2011), 969–988.

Sirgue, L., and R. G. Pratt: Efficient waveform inversion and imaging: A strategy for selecting temporal frequency, *Geophysics*, **69**, (2004), 231–248.

Tan, S., and L. Huang: An efficient finite-difference method with high-order accuracy in both time and space domains for modelling scalar-wave propagation, *Geophysical Journal International*, **197**, (2014), 1250–1267.

Tan, S., and L. Huang: A staggered-grid finite-difference scheme optimized in the time–space domain for modeling scalar-wave propagation in geophysical problems: *Journal of Computational Physics*, **276**, (2014), 613–634.

Tarantola, A.: Inversion of seismic reflection data in the acoustic approximation, *Geophysics*, **49**(8), (1984), 1259-1266.

Virieux, J., and Operto, S.: An overview of full-waveform inversion in exploration geophysics, *Geophysics*, **74**(6), (2009), WCC1-WCC26.